Topological Insulators and the Bulk–Boundary Correspondence

Yiyang Jiang
Department of Physics, The Pennsylvania State University

Topology Seminar · June 30, 2026

Abstract. These notes build the bulk–boundary correspondence of topological band insulators from the ground up: the modern theory of polarization and the position operator in the Bloch basis; the quantized Hall conductivity obtained three equivalent ways (adiabatic pump, Kubo response, Boltzmann anomalous velocity) and recast as a Berry-curvature / Chern-number topology via the Gauss map of the Brillouin zone onto the Bloch sphere; the integer quantum Hall system as the first topological insulator, with confinement-induced chiral edge modes and the velocity-cancellation pinning $\sigma_{xy} = e^2/h$; the rigorous Dirac (Jackiw–Rebbi) and Wilson-loop derivations of the protected edge spectrum; and the wider topological zoo (2D/3D topological insulators, Weyl semimetals and Fermi arcs, higher-order phases). All illustrations are redrawn in Python.

I. Review of the Last Lecture

Review of last Lecture

- Bloch Band Theory

$$\begin{cases}\text{Plane Wave Expansion}\\ \text{Tight binding Approximation}\end{cases} \tag{1}$$

- Modern Theory of Polarization

$$A_n = \langle u_n|\, i\nabla_k\, |u_n\rangle \tag{2}$$

Duality between position and crystal-momentum operators:

$$\hat{r} \;\longleftrightarrow\; \hat{k} \sim i\nabla_r \tag{3}$$

Matrix element of the position operator between Bloch states:

$$\begin{aligned} r_n &= \langle\psi_{nk'}|\,\hat{r}\,|\psi_{nk}\rangle = \langle u_{nk'}|\, e^{-ik'\hat{r}}\,\hat{r}\, e^{ik\hat{r}}\,|u_{nk}\rangle \\ &= \langle u_{nk'}|\, e^{-ik'\cdot r}\,\left(-i\,\nabla_k\,(e^{ik\cdot r})\right)|u_{nk}\rangle \\ &= \langle\psi_{nk'}|-i\nabla_k\,|\psi_{nk}\rangle \;+\; i\,\langle u_{nk'}|\,e^{-ik'\cdot r}\,e^{ik\hat{r}}\,|\nabla_k u_{nk}\rangle \\ &= i\nabla_k\langle\psi_{nk'}|\psi_{nk}\rangle \\ &= i\nabla_k\,\delta(k-k') \;+\; A_n(k) \end{aligned} \tag{4}$$

8

$$\begin{aligned} j_y &= \frac{dP^y}{dt} = \frac{d}{dt}\left(e\sum_{occ.}\int_k\langle\psi_{nk}|\,\hat{y}\,|\psi_{nk}\rangle\right) \\ &= \frac{d}{dt}\left(\sum_{occ.}\int_k A^y_{nk}\right) \end{aligned} \tag{9}$$

$$k \;\to\; k + \frac{eE}{\hbar}\,t \tag{10}$$

Analysis note (sign in the r_n derivation). Writing $|\psi_{nk}\rangle = e^{ik\hat{r}}|u_{nk}\rangle$ and using $\hat{r}\,e^{ik\hat{r}} = -i\nabla_k\,e^{ik\hat{r}}$, the product rule

$$\nabla_k(e^{ikr}|u_{nk}\rangle) = (\nabla_k e^{ikr})|u_{nk}\rangle + e^{ikr}|\nabla_k u_{nk}\rangle \tag{11}$$

splits r_n into a "diagonal" piece $\propto \nabla_k\langle\psi_{nk'}|\psi_{nk}\rangle = \nabla_k\delta(k-k')$ and the Berry connection $A_n(k) = \langle u_{nk}|\,i\nabla_k\,|u_{nk}\rangle$. The position operator in the Bloch basis is therefore $i\nabla_k$ plus the Berry connection — this is the content of the Modern Theory of Polarization, and it is why the polarization $P = \sum_{occ.}\int_k A_{nk}$ is only defined modulo a lattice constant (gauge / r_0 freedom).

Continuing the Hall-current derivation. The time-dependence enters only through the drifting crystal momentum:

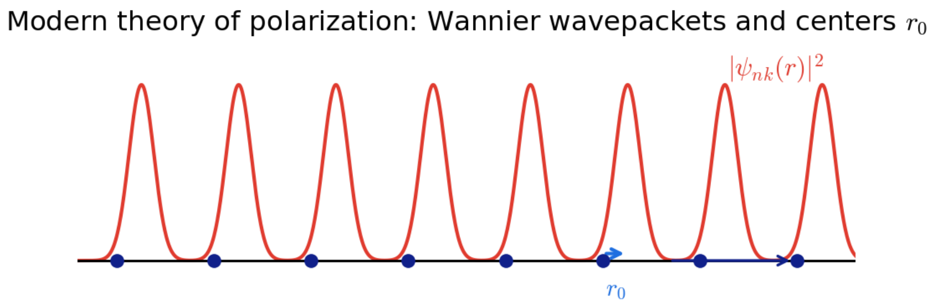

Figure 1. Periodic array of Wannier wavepackets; the polarization is set by the center r_0 of |ψ_nk(r)|^2.

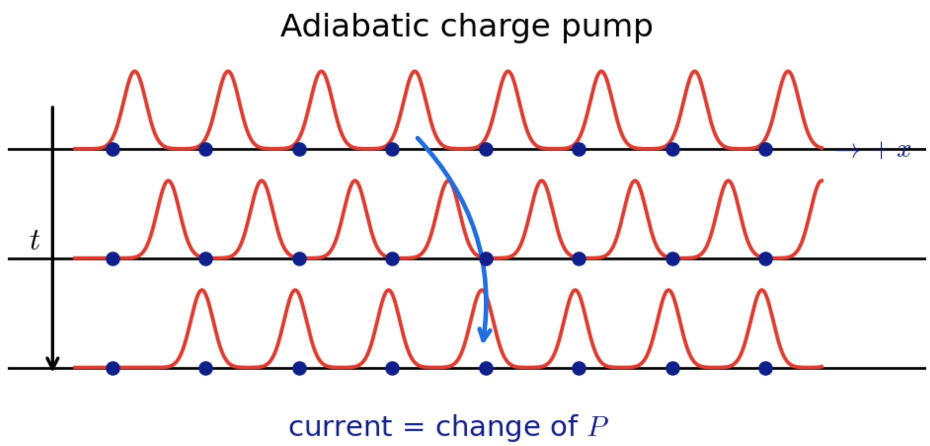

Figure 2. Adiabatic pump: as the parameter t advances (top to bottom), each occupied wavepacket slides by +x; the flowing charge equals the change of the polarization P.

$$\frac{d}{dt}|\psi_{nk}\rangle = |\partial_{k_x}\psi_{nk}\rangle \frac{dk_x}{dt}, \qquad \frac{dk_x}{dt} = \frac{eE_x}{\hbar} \tag{12}$$

$$\begin{aligned} j_y &= \sum_{occ.} \int_k \left(\partial_{k_x} A^y - \partial_{k_y} A^x\right) \frac{eE_x}{\hbar} \\ &= \left(\sum_{occ.} \int_k \Omega^{xy}\right) \frac{eE_x}{\hbar} \end{aligned} \tag{13}$$

with the Berry curvature

$$\Omega^{xy} = \langle \partial_{k_x} u_{nk} | \partial_{k_y} u_{nk} \rangle - (x \leftrightarrow y) \tag{14}$$

Quantized Hall conductivity:

$$\sigma_H = \frac{e^2}{\hbar} \int d^2k\, \Omega = \int_{\text{Bloch}} dS = C \in \mathbb{Z} \quad \longleftarrow \textbf{Topology} \tag{15}$$

(area element on the Bloch sphere: $\Omega\, dk_x\, dk_y$.)

Topology: this doesn't change under continuous / smooth perturbation.

A. Kubo Formalism

$$\sigma_{xy} = \int d^2k \, \frac{\langle u_m | \frac{\partial H}{\partial k_x} | u_n \rangle \langle u_n | \frac{\partial H}{\partial k_y} | u_m \rangle}{(\varepsilon_n - \varepsilon_m)^2} \tag{16}$$

$$= \int d^2k\, \Omega^{xy} \tag{17}$$

$$\partial_t f + eE \cdot \nabla_k f = \frac{f - f_0}{\tau} \tag{18}$$

B. Boltzmann Transport

(distributions: $f(E^0)$ and $f(E^1)$)

$$j = \int f \cdot v \tag{19}$$

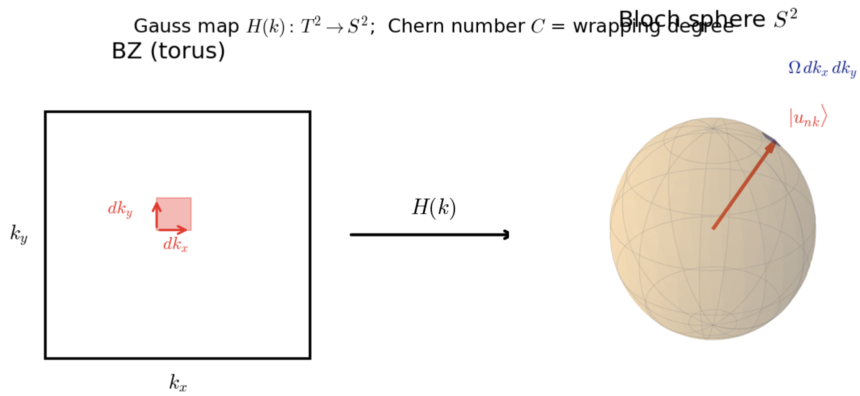

Figure 3. The Bloch Hamiltonian H(k) maps the BZ (a square / torus, area element dk_x dk_y) to the Bloch sphere; |u_nk⟩ traces out the sphere and the Berry curvature Ω dk_x dk_y is the pulled-back area. The Chern number C is the number of times the BZ wraps the sphere.

$$v_n = \underbrace{\frac{\partial \varepsilon_n}{\partial k}}_{(E^0)} + eE \times \Omega \tag{20}$$

The anomalous-velocity piece gives the boxed intrinsic Hall current $\int f\, eE \times \Omega$. Expanding $j = \int f\, v$ to first order in E:

$$j(E^1) = f^{(1)} v^{(0)} + \boxed{f^{(0)} v^{(1)}} \tag{21}$$

where

$$\begin{aligned} f^{(1)} &= eE\tau\, \nabla_k f^{(0)} \\ v^{(0)} &= \frac{\partial \varepsilon}{\partial k} \end{aligned} \tag{22}$$

$$j_{\text{Drude}} = eE\tau \int_k (\nabla_k f)(\nabla_k \varepsilon) \tag{23}$$

Analysis note (the three equivalent routes to σ_H). The page lays the *quantized* Hall conductance next to three derivations that all return the same Berry-curvature integral: (i) the polarization-current / adiabatic argument of Page 1, $\sigma_H = \frac{e^2}{\hbar} \int_{BZ} \Omega$; (ii) the **Kubo** linear-response formula, whose sum over virtual interband transitions $\frac{\langle m|\partial_{k_x} H|n\rangle\langle n|\partial_{k_y} H|m\rangle}{(\varepsilon_n - \varepsilon_m)^2}$ is exactly Ω^{xy} after taking the imaginary part; (iii) the semiclassical **Boltzmann** equation with the anomalous velocity $eE \times \Omega$, which separates the longitudinal Drude term ($f^{(1)} v^{(0)}$) from the transverse intrinsic term ($f^{(0)} v^{(1)}$). The factor written as $\frac{e^2}{\hbar}$ becomes the quantum of conductance $\frac{e^2}{h}$ once the $\frac{1}{2\pi}$ of $\int_k = \int \frac{d^2k}{(2\pi)^2}$ is restored, so that $C = \frac{1}{2\pi} \int_{BZ} \Omega\, d^2k \in \mathbb{Z}$. The map $H(k) : T^2 \to S^2$ makes C a topological degree (Gauss map): it counts how many times the Brillouin torus wraps the Bloch sphere and is therefore invariant under any smooth deformation that keeps the gap open.

Finishing the Drude conductivity from the previous step. Integrating by parts ($\nabla_k f \to f\, \nabla_k$) and using $\varepsilon = \frac{\hbar^2 k^2}{2m}$:

$$\begin{aligned} j_{\text{Drude}} &= eE\tau \int_k f\, (\partial_k \partial_k \varepsilon) \\ &= \frac{eE}{m^*} \tau \boxed{\int f} \\ &= \frac{neE}{m^*} \tau \end{aligned} \tag{24}$$

(here $\partial_k \partial_k \varepsilon = 1/m^*$ is the inverse effective mass, and $\int f = n$ the carrier density.)

II. Bulk–Boundary Correspondence (BBC)

Band picture under a field. Conduction band CB (parabola), occupied states drawn shaded; with an applied E_x the occupation is displaced so that $\frac{\partial \varepsilon}{\partial k_x} > 0 \Rightarrow v_x > 0$.

The valence band VB below carries the **bulk** states; in the gap, **surface** states appear (drawn in blue) — the hallmark of bulk–boundary correspondence.

Bulk — Landau problem (minimal coupling / Peierls substitution):

$$H = H(p \to p + eA) \tag{25}$$

$$\vec{B} = \nabla \times \vec{A}, \qquad \vec{A} = -Bx\,\hat{y} \quad \text{(Landau gauge)} \tag{26}$$

The bulk Hamiltonian becomes

$$H = \frac{(p_y - Bx)^2 + p_x^2}{2m} \tag{27}$$

(equivalently $\propto (x - \frac{p_y}{B})^2$, a shifted harmonic oscillator), with eigenfunctions

$$\psi_{n,k} = e^{ik_y y} H_n(x - k_y \ell_B^2) \tag{28}$$

where H_n is the Hermite function and ℓ_B the magnetic length. The spectrum is a ladder of flat **Landau levels**

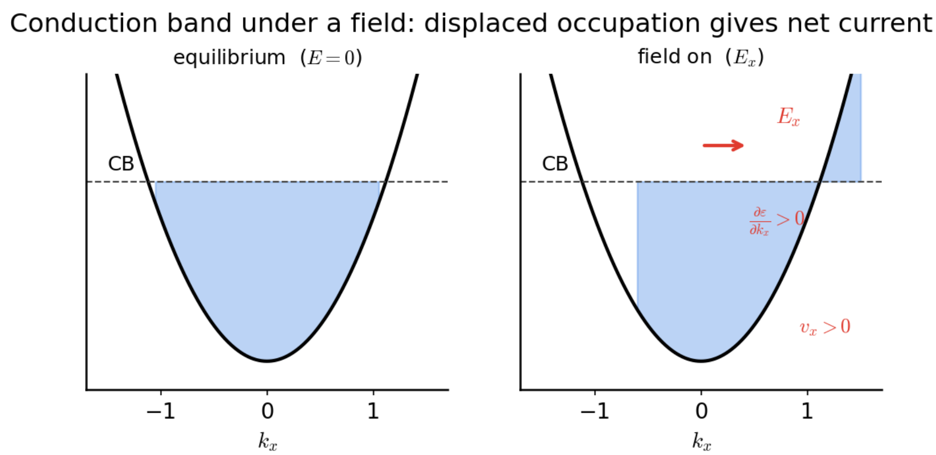

Figure 4. Conduction-band parabola (CB). At equilibrium the filled states are symmetric (no net current); an applied field E_x displaces the occupation so $\partial\varepsilon/\partial$k_x > 0 and v_x > 0 — the Drude/Boltzmann current.

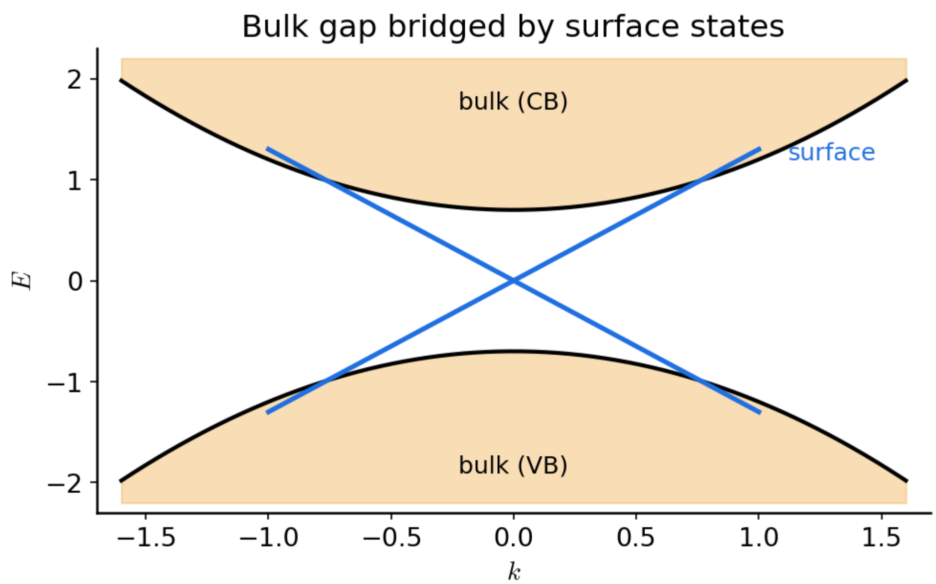

Figure 5. Bulk valence/conduction bands (shaded) with in-gap surface/edge states (blue) crossing the bulk gap — the bulk–boundary correspondence.

$$E_n = \left(n + \tfrac{1}{2}\right)\hbar\omega_c \tag{29}$$

each massively degenerate. Degeneracy:

$$D = \frac{S}{\pi\,\ell_B^2} \quad \left(= \frac{L_x L_y}{2\pi\,\ell_B^2}\right) \tag{30}$$

Boundary. Add a confining potential:

$$H = H_{\text{bulk}} + V(x), \qquad V(x) = \begin{cases} 0 & \text{bulk} \\ \infty & \text{outside} \end{cases} \tag{31}$$

Because the n-th eigenstate is localized at the guiding center $x = k_y\ell_B^2$ (its density $\approx \delta(x - k_y\ell_B^2)$), the energy in the presence of the wall is

$$\begin{aligned} E &= \langle\psi|H|\psi\rangle \\ &= \langle\psi|H_{\text{bulk}}|\psi\rangle + \langle\psi|V(x)|\psi\rangle \\ &= \left(n + \tfrac{1}{2}\right)\hbar\omega_c + V(k_y\ell_B^2) \end{aligned} \tag{32}$$

with $\langle\psi|V|\psi\rangle = \int \psi^*(x)\,V(x)\,\psi(x)\,dx \approx V(k_y\ell_B^2)$. In the bulk the levels stay flat, but near each wall $V(k_y\ell_B^2)$ bends them upward, giving dispersing **edge states** with

$$v_y = \frac{\partial E}{\partial k_y} \tag{33}$$

On opposite edges the slope has opposite sign: $\frac{\partial E}{\partial k_y} < 0$ on one boundary and $\frac{\partial E}{\partial k_y} > 0$ on the other — i.e. counter-propagating **chiral** modes. (Allowed momenta are quantized by the sample size, $\Delta k_y = 2\pi/L_y$.)

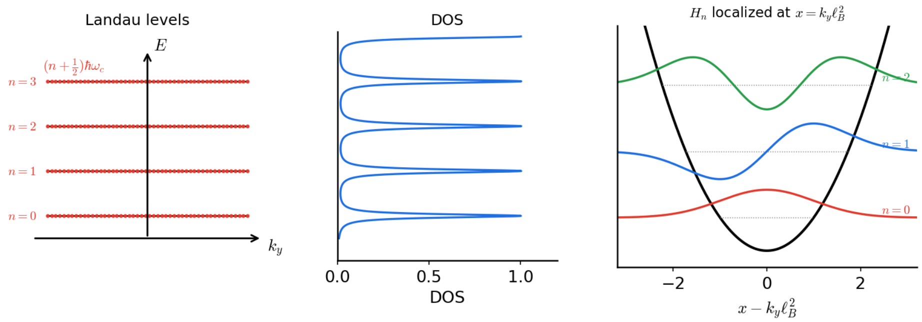

Figure 6. Bulk Landau levels: flat E_n=(n+½)$\hbar\omega$_c versus k_y (left), the corresponding spiky density of states (center), and the shifted harmonic-oscillator eigenfunctions H_n centered at x = k_y ℓ_B^2 (right).

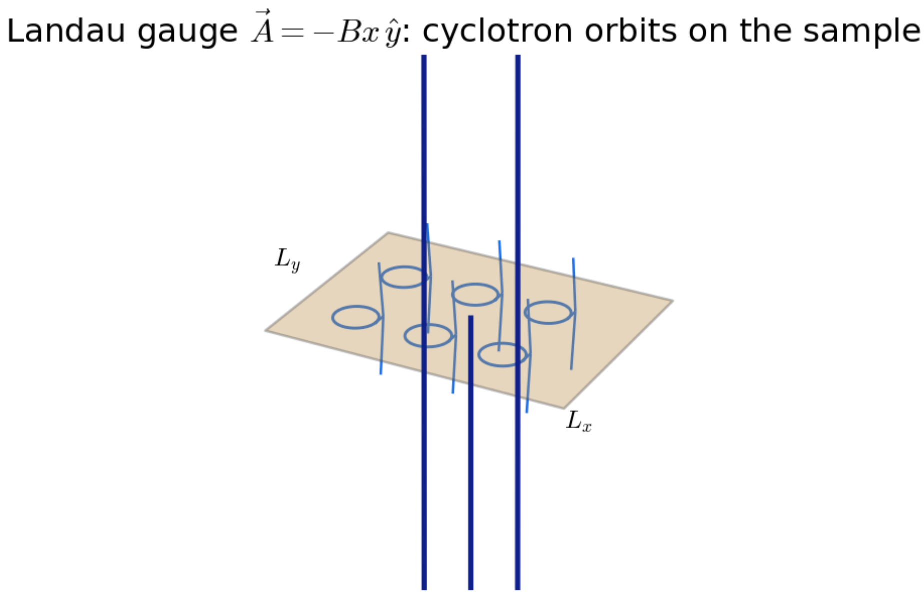

Figure 7. Landau gauge picture: a 2D sample (the L_x×L_y plane) in a perpendicular field B = ∇×A with A = −Bx $\hat{y}$; electrons execute cyclotron orbits whose guiding centers tile the plane.

Analysis note (why edges force gapless modes). Each filled bulk Landau level contributes one chiral edge branch per boundary. Where a branch crosses the Fermi level it must do so with a definite sign of $v_y = \partial_{k_y} E$, and the two boundaries carry opposite signs, so the net edge current is non-zero and quantized. The number of such crossings equals the Chern number C of the filled bands — this is the microscopic statement of bulk–boundary correspondence: $\#(\text{chiral edge modes}) = C = \frac{1}{2\pi}\int_{BZ} \Omega\, d^2k$. The guiding-center relation $x = k_y \ell_B^2$ is what ties a bulk quantum number (k_y) to a real-space position (x), turning the bulk topological index into a boundary spectral feature.

Edge spectrum in the gap. The two bulk bands are separated by a gap; the confinement makes the edge branches disperse linearly and **cross** inside the gap (a 1D Dirac crossing), one branch with $\frac{\partial E}{\partial k_y} < 0$ and one with $\frac{\partial E}{\partial k_y} > 0$. The density of states shows these in-gap **surface states**, and the edge velocity is tied to the slope of the confining wall:

$$\frac{\partial E}{\partial k_y} \sim \frac{\partial V}{\partial x} \tag{34}$$

Why must this crossing be there, model-independently? Because the low-energy physics at *any* TI boundary is a **Dirac mass that changes sign** (Jackiw–Rebbi). Take the BHZ model

$$H(k_x, k_y; u) = \sin k_x\, \sigma_x + \sin k_y\, \sigma_y + (u + \cos k_x + \cos k_y)\, \sigma_z, \tag{35}$$

trivial for $u < -2$ and a Chern insulator ($C = -1$) for $-2 < u < 0$; the gap closes at $\Gamma = (0,0)$. Expanding there gives a (2+1)D Dirac fermion

$$H \approx k_x\sigma_x + k_y\sigma_y + m\,\sigma_z, \qquad m \equiv u + \cos k_x + \cos k_y \approx u + 2. \tag{36}$$

A boundary at $x = 0$ (interior $x < 0$, vacuum/trivial $x > 0$) is exactly where the mass reverses, $m(x) > 0$ ($x < 0$) and $m(x) < 0$ ($x > 0$). Keeping k_y good and setting $k_x \to -i\partial_x$,

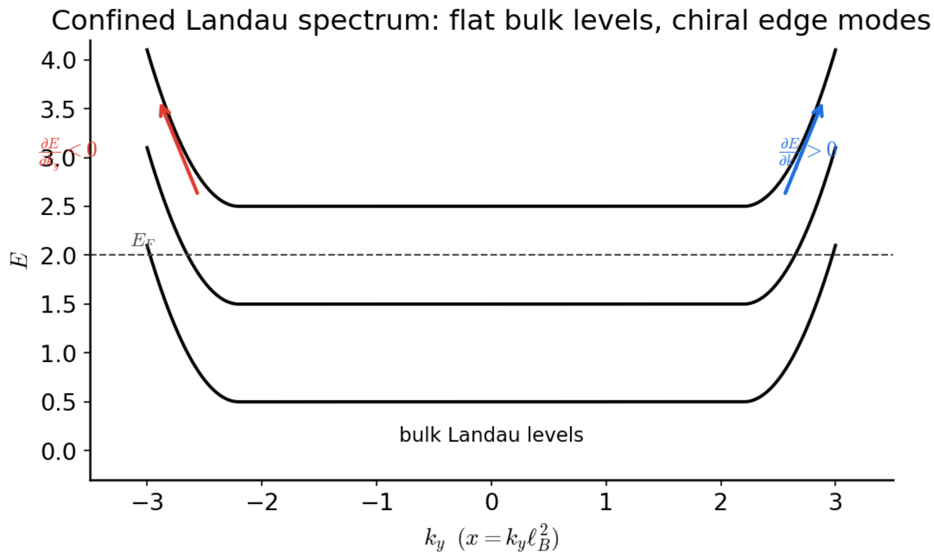

Figure 8. Confined Landau spectrum: bulk levels stay flat at (n+½)ℏω_c, but the edge potential V(x) bends them up near both walls, producing chiral edge modes with v_y = ∂E/∂k_y of opposite sign on the two boundaries.

$$H(x, k_y) = -i\sigma_x \partial_x + k_y \sigma_y + m(x)\sigma_z. \tag{37}$$

At $k_y = 0$, using $\sigma_x \sigma_z = -i\sigma_y$,

$$-i\sigma_x \partial_x \Psi = -m(x)\sigma_z \Psi \implies \partial_x \Psi = -m(x)\,\sigma_y\,\Psi, \tag{38}$$

so Ψ is a σ_y eigenstate, $\Psi^\pm = \psi^\pm(x)\binom{1}{\pm i}$ with $\partial_x \psi^\pm = \mp m(x)\psi^\pm$, i.e. $\psi^\pm \propto e^{\mp\int^x m\,dx'}$. Only one sign is normalizable (the mass reversal binds a single chirality), giving the zero mode

$$\Psi_{k_y=0}(x) = \mathcal{N}\, e^{-\int^x m(x')\,dx'} \begin{pmatrix} 1 \\ -i \end{pmatrix}, \qquad E(k_y{=}0) = 0. \tag{39}$$

Restoring k_y, the $k_y\sigma_y$ term acts on the σ_y eigenspinor as a c-number, so the bound state disperses linearly,

$$E(k_y) = k_y, \tag{40}$$

a **gapless chiral edge mode** — precisely the crossing in the figure, now rigorous. A smooth ramp $m(x) = -\alpha x$ localizes it as a Gaussian $\Psi_0 \propto e^{-\alpha x^2/2}$ at $x = 0$; a sharp mass step gives an exponentially localized packet. This is why the tight-binding numerics only ever *verify* the correspondence (PBC → gapped bulk; OBC → gapless in-gap branch) — the sign-changing Dirac mass is what actually *forces* it.

Hall bar. Put the sample in a field E (driven by a battery injecting e^-). The top ($+y$) and bottom ($-y$) edges carry the two chiral channels. In steady state the electrochemical potential is flat:

$$\mu(x) + eEx = \text{Const} \tag{41}$$

so the two edges sit at different chemical potentials, with

$$\Delta\mu \propto E \tag{42}$$

i.e. a transverse (Hall) voltage $\Delta\mu = eV$.

Edge current. Count the occupied edge states in the bias window and add up the current they carry. The allowed k_y are spaced by $\Delta k_y = \frac{2\pi}{L_y}$, and a single edge state circulating a ring of circumference L_y at velocity v_y carries current $\dfrac{e\,v_y}{L_y}$, with

$$v_y = \frac{1}{\hbar}\frac{\partial E}{\partial k_y} \tag{43}$$

The bias window set by the longitudinal drop is $\Delta\mu = eE_x L_x$, and the energy spacing between adjacent edge states is $\delta E = \dfrac{\partial E}{\partial k_y}\,\Delta k_y = \dfrac{\partial E}{\partial k_y}\dfrac{2\pi}{L_y}$, so the number of current-carrying states is

$$\Delta N = \frac{\Delta\mu}{\delta E} = \frac{eE_x L_x}{\dfrac{\partial E}{\partial k_y}\cdot\dfrac{2\pi}{L_y}} = \frac{eE_x L_x L_y}{2\pi\,\dfrac{\partial E}{\partial k_y}} \tag{44}$$

The total edge current is then

$$I_y = \Delta N \cdot \frac{e\,v_y}{L_y} = \frac{eE_x L_x L_y}{2\pi\,\frac{\partial E}{\partial k_y}} \cdot \frac{e}{L_y} \cdot \frac{1}{\hbar}\frac{\partial E}{\partial k_y} \tag{45}$$

Both the band velocity $\dfrac{\partial E}{\partial k_y}$ and the system size L_y cancel:

$$I_y = \frac{e^2 E_x L_x}{2\pi\hbar} = \frac{e^2}{h}\,E_x L_x \tag{46}$$

Converting to a current density (current per transverse width L_x) and reading off the conductivity:

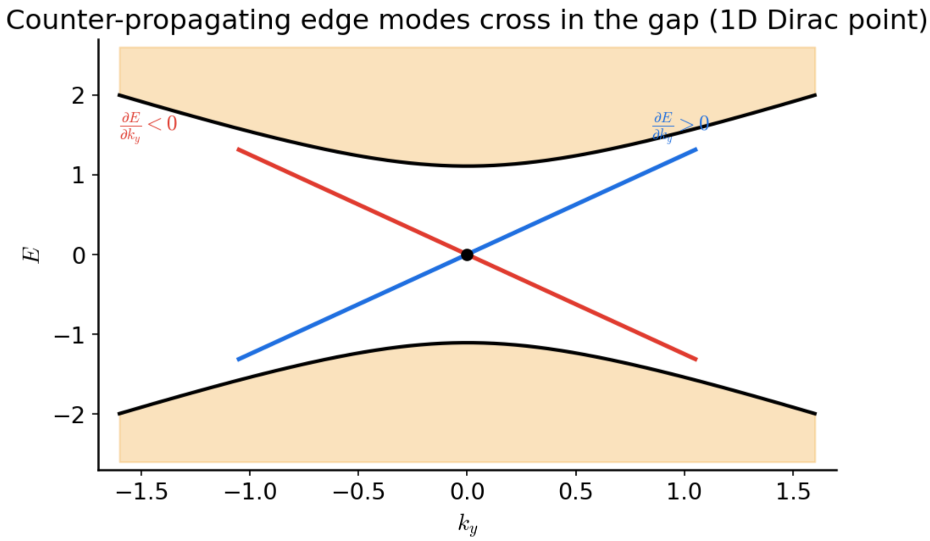

Figure 9. Edge spectrum: the bulk valence and conduction bands (shaded) leave a gap, bridged by two counter-propagating edge branches that cross linearly (1D Dirac point). Left branch ∂E/∂k_y < 0, right branch ∂E/∂k_y > 0; the in-gap DOS is the surface state.

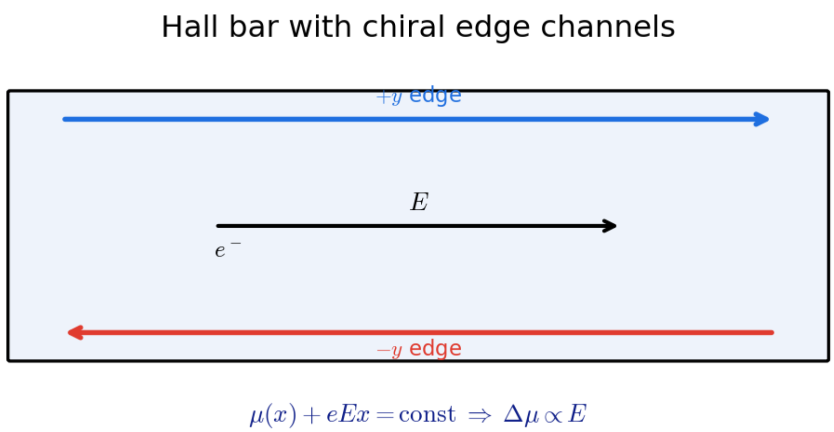

Figure 10. Hall bar with one chiral edge channel on each long side (−y edge in red, +y edge in blue). A battery drives e⁻ through a longitudinal field E; the constraint μ(x)+eEx=const forces a chemical-potential difference $\Delta\mu \propto$ E between the two edges — the Hall voltage.

$$j_y = \frac{I_y}{L_x} = \frac{e^2}{h} E_x, \qquad \sigma_{xy} = \frac{j_y}{E_x} = \frac{e^2}{h} \tag{47}$$

Analysis note (correcting the raw derivation → quantization). The handwritten page writes the current per state as $e\,v_y$ and ends at $\sigma_{xy} = e^2/\hbar$, which leaves a spurious factor of L_y and an extra 2π. Two corrections fix it. (i) A single state on a ring of circumference L_y carries current $e\,v_y/L_y$, not $e\,v_y$ — the missing $1/L_y$ cancels the L_y coming from ΔN. (ii) $v_y = \frac{1}{\hbar}\partial_{k_y} E$, so the $\hbar$ combines with the 2π from $\Delta k_y = 2\pi/L_y$ into $h = 2\pi\hbar$. The non-universal band velocity $\partial_{k_y} E$ appears once downstairs (in ΔN) and once upstairs (in v_y) and **cancels exactly**, leaving $\sigma_{xy} = \nu\,\dfrac{e^2}{h}$, with ν = number of edge channels crossing the Fermi level = Chern number. The cancellation of every material-specific quantity (velocity, size, level spacing) is the signature of a topological response.

A. The Quantum Hall Effect as the First Topological Insulator

Before generalizing, it is worth consolidating the prototypical example in full. The integer quantum Hall system is the original **topological insulator**: a gapped, fully-filled bulk that is nevertheless forced to carry gapless chiral states at its boundary — the simplest instance of bulk–edge correspondence, with the topology showing up as a quantized response. Throughout, l_B is the magnetic length, $\omega_c = eB/mc$ the cyclotron frequency, and Φ_0 the flux quantum.

1. Landau levels: the gapped bulk

Work in the **Landau gauge**

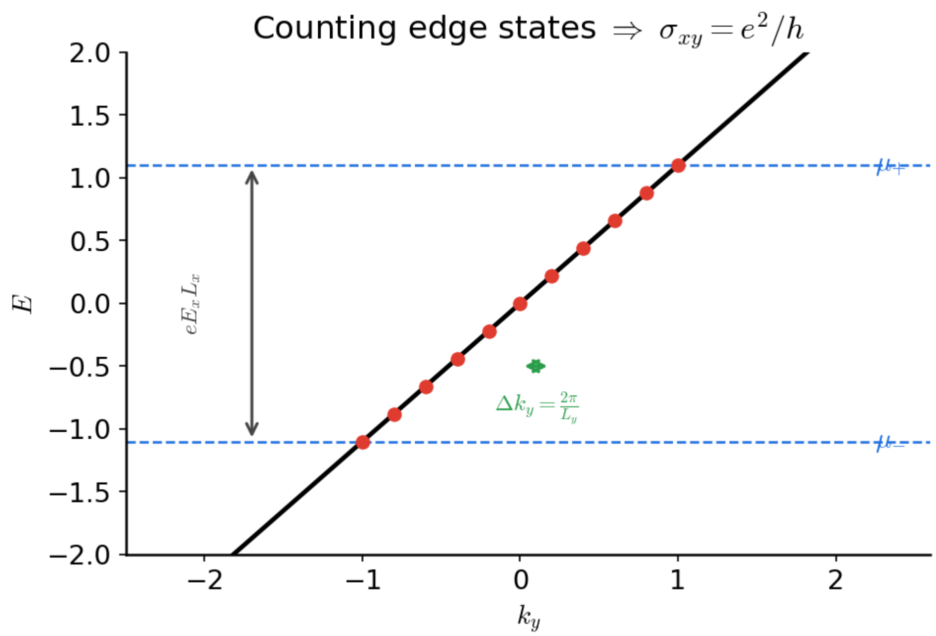

Figure 11. Edge dispersion filled up to the local chemical potential μ(x): occupied states (dots) are spaced by Δk_y = 2π/L_y. The ΔN states in the bias window eE_xL_x each carry e v_y/L_y; the velocity cancels the level spacing and the L_y cancels, leaving σ_xy = e^2/h.

$$A = -Bx\,\hat{y} \qquad \text{(breaks } x\text{-translation symmetry).} \tag{48}$$

(In the symmetric gauge one is led instead toward the FQHE.) The single-particle Hamiltonian is

$$H = \frac{\left(p_y - \frac{e}{c}Bx\right)^2 + p_x^2}{2m}. \tag{49}$$

Because y-translation is preserved, k_y is a good quantum number and the eigenstates are plane waves along y times harmonic-oscillator states in x, centered at the guiding center $x = k_y l_B^2$:

$$\psi_{n,k_y}(x,y) = e^{ik_y y}\, H_n\!\left(x - k_y l_B^2\right). \tag{50}$$

The spectrum is the ladder of **Landau levels**, independent of k_y,

$$\varepsilon_{n,k_y} = \left(n + \tfrac{1}{2}\right)\hbar\omega_c, \tag{51}$$

each macroscopically degenerate and localized in x about $x = k_y l_B^2$. The density of states is a set of sharp peaks separated by **gaps**.

The degeneracy per level equals the number of flux quanta threading the sample,

$$D = \frac{\text{Area} \cdot B}{\Phi_0}. \tag{52}$$

When an integer number of Landau levels is **fully filled**, the system is an **insulator** (filled and gapped). (If instead a flat level is only partially filled — filling fractions $\nu = \frac{1}{3}, \frac{1}{5}, \ldots$ where the interaction energy dominates the kinetic energy, $E_{\text{int}} \gg E_{\text{kin}}$ — one enters the **FQHE** regime.)

2. *Confinement and the chiral edge*

Add a slowly varying confining potential, $H = H_{\text{bulk}} + V(x)$. For a slowly changing $V(x)$, each state localized at $x_0 = k_y l_B^2$ simply picks up the local potential value, so the levels acquire a k_y-dependence,

$$\varepsilon_{n,k_y} = \left(n + \tfrac{1}{2}\right)\hbar\omega_c + V\!\left(k_y l_B^2\right). \tag{53}$$

In the bulk the levels stay flat (dispersionless), but near each boundary they bend upward following $V(x)$ and cross the Fermi level, producing **chiral edge states**. On one edge the group velocity is negative ($v_y < 0$); on the opposite edge it is positive — the two edges carry counter-propagating currents. The bulk remains **gapped** while the edges are **gapless** — the prototypical bulk–edge correspondence.

3. *Anatomy of the chiral edge mode*

The edge mode is (i) **localized** at the edge, (ii) **chiral**, and (iii) understood semiclassically as a *skipping orbit*: with the field B out of the plane ($\odot B$), electrons in the bulk execute closed cyclotron orbits, while at the boundaries they skip along the edge. The two edges carry opposite velocities, $v_y < 0$ on the left edge and $v_y > 0$ on the right.

It is (iv) **robust**. A *bulk impurity* only changes the local shape of $V(x)$ (a dip in the potential); the chiral edge channel is unaffected. An *edge impurity* only changes the boundary shape; the skipping orbits simply follow the deformed boundary around the impurity, so the chiral mode cannot backscatter.

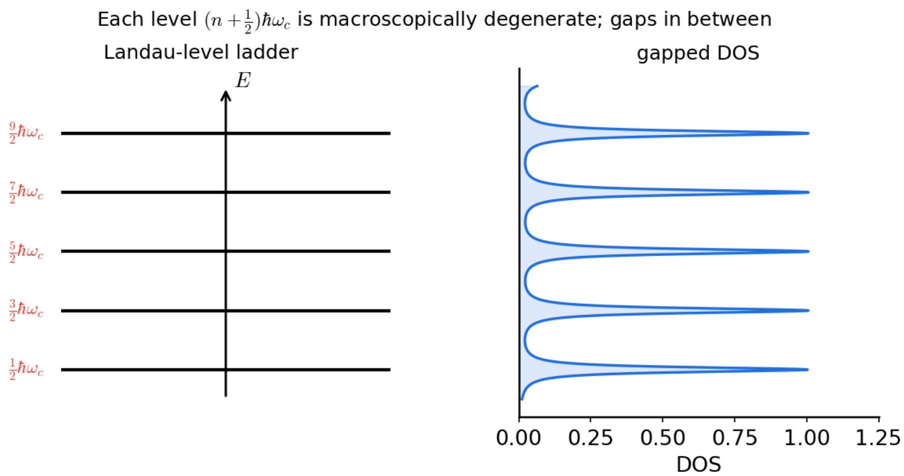

Figure 12. Landau-level ladder (½, 3/2, 5/2 … $\hbar\omega$_c), each highly degenerate, with a gapped density of states

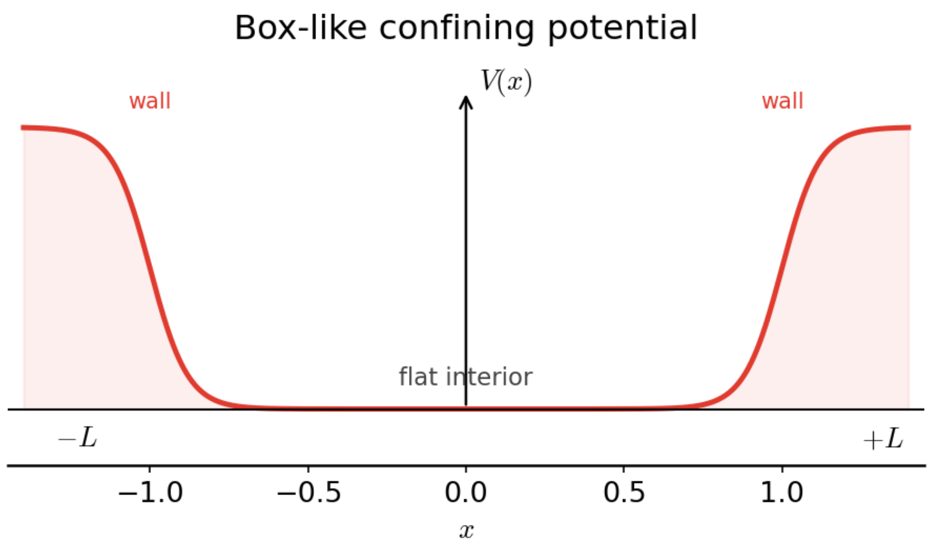

Figure 13. Box-like confining potential V(x): flat in the interior with steep walls at the two boundaries

Finally, it produces a (v) **quantized response**. Apply a voltage U across the sample (a difference $\Delta\mu = eU$ between the two edges); with B out of plane, the Hall current J_{Hall} flows transverse to it.

The number of current-carrying states between the two chemical potentials is

$$\Delta N = \frac{U}{\left(\frac{\partial E}{\partial k_y}\right)\left(\frac{\partial k_y}{\partial N}\right)}, \tag{54}$$

with edge-state group velocity $v_y = \partial E/\partial k_y$ and Landau-level degeneracy (total number of states) $N_{\text{tot}} = AB/\Phi_0$, so the k_y-spacing follows as $\partial k_y/\partial N = (\,?\,)/(AB/\Phi_0)$. Putting these together, the **Hall current**, **current density**, and **Hall conductivity** are

$$I_y = \Delta N\, e\, v_y = \frac{eU}{2\pi/L_y}\cdot\frac{AB}{\Phi_0}, \qquad j_y = \frac{I_y}{L_x}, \qquad \sigma_{xy} = \frac{j_y}{E_x} = \frac{I_y/L_x}{U/L_x} = \frac{e^2}{h}. \tag{55}$$

Analysis note. This is the standard counting argument for the quantized Hall conductance of a single filled Landau level: each filled level contributes one chiral edge channel carrying e^2/h. The intermediate factor $\partial k_y/\partial N$ is flagged with "(?)" (an unresolved bookkeeping step in the lecture), and the velocity is written with $\hbar = 1$ ($v_y = \partial E/\partial k_y$).

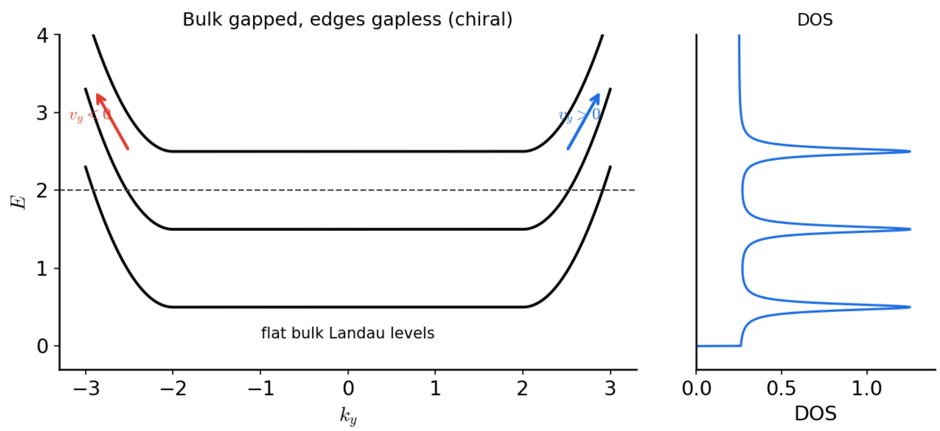

Figure 14. E vs k_y: flat bulk Landau levels bending up into chiral edge states at the two boundaries; DOS gapped in the bulk and gapless at the edges

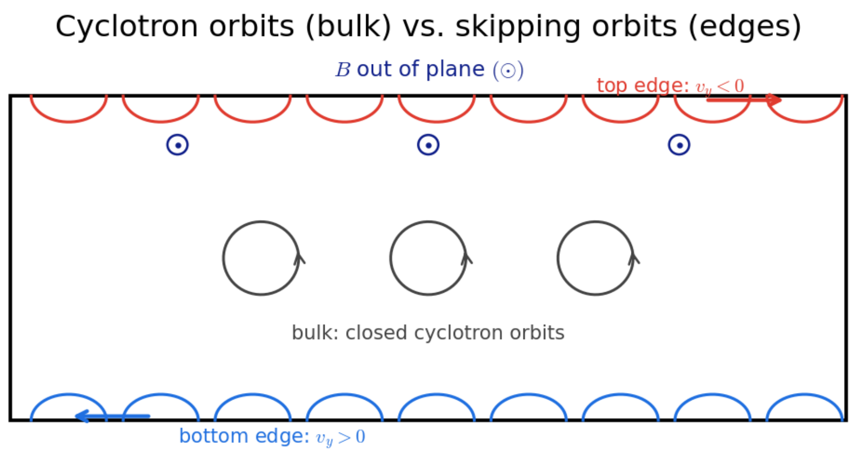

Figure 15. Cyclotron picture: closed orbits in the bulk, skipping orbits along the two edges with opposite v_y

The endpoint $\sigma_{xy} = e^2/h$ is the quantized response, robust because it counts edge channels — the same velocity-cancellation seen in the main edge-counting derivation.

4. *Other quantized responses*

The same one-dimensional cancellation quantizes several transport coefficients. For the **electric conductivity**,

$$I = e\int_{\mu_1}^{\mu_2} dE\,\mathrm{DOS}(E)\,v(E), \tag{56}$$

and in 1D $\mathrm{DOS}(E) \propto 1/|\partial E/\partial k|$ while $v(E) = \partial E/\partial k$, so the product $\mathrm{DOS}(E)\,v(E)$ is a constant — the band-structure details cancel, giving

$$I = \frac{e}{h}(\mu_2 - \mu_1) = \frac{e^2}{h}V. \tag{57}$$

For the **thermal conductivity**,

$$I^T = \int_{-\infty}^{+\infty} dE\,E\,\mathrm{DOS}(E)\,v(E)\,\frac{\partial f}{\partial T}\,(T_2 - T_1) = \frac{\pi^2}{3}\,\frac{T}{h}\,\Delta T, \tag{58}$$

so by the same cancellation the thermal conductance is also quantized, with quantum of thermal conductance $\frac{\pi^2}{3}\frac{k_B^2 T}{h}$ (here $k_B = 1$).

5. *Experiment*

Contrasting (ρ_{xx}, ρ_{xy}) versus B: in the **classical** Hall effect ρ_{xy} is linear in B and ρ_{xx} roughly constant, whereas in the **quantum** regime ρ_{xy} develops quantized plateaus while ρ_{xx} collapses to zero between peaks (the integer quantum Hall staircase). A recent measurement of quantum-Hall edge struc-

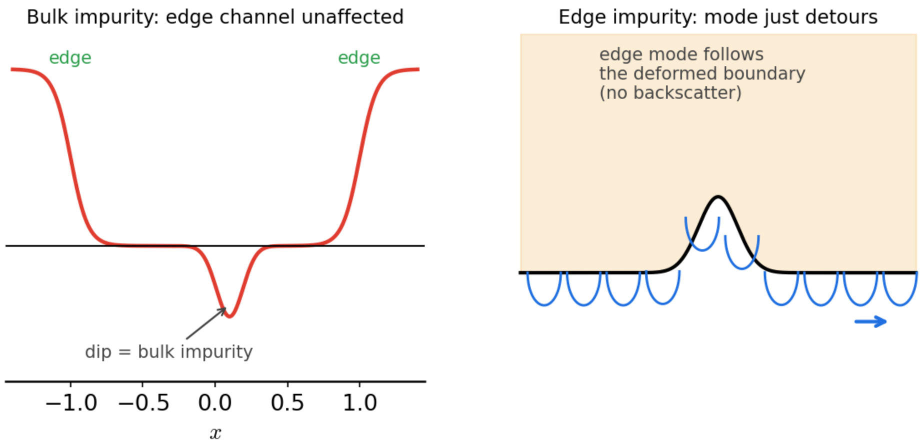

Figure 16. Robustness: a bulk impurity is a dip in V(x); an edge impurity just reshapes the boundary the edge mode follows

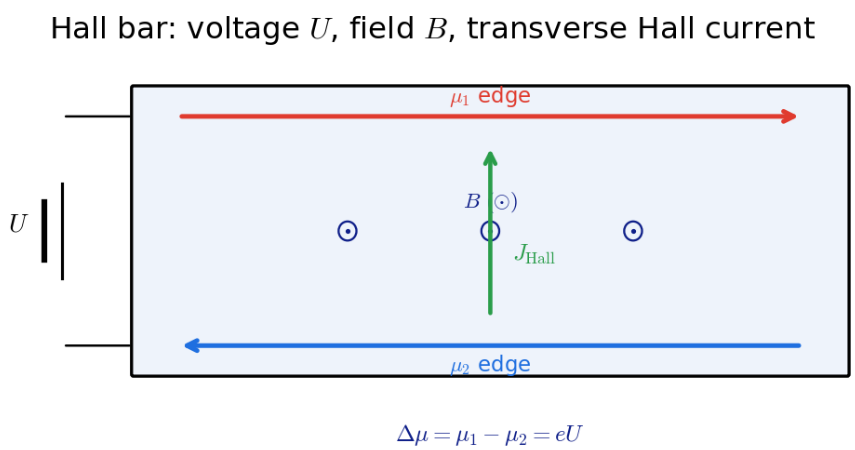

Figure 17. Hall-bar geometry: voltage U applied, B out of plane, Hall current flowing transverse, with chemical potentials μ_1, μ_2 on the two edges

ture illustrates this physics:

> **nature** — Article, published 17 December 2025. "Visualizing interaction-driven restructuring of quantum Hall edge states." Jiachen Yu, Haotan Han, Kristina G. Wolinski, Ruihua Fan, Amir S. Mohammadi, Tianle Wang, Taige Wang, Liam Cohen, Kenji Watanabe, Takashi Taniguchi, Andrea F. Young, Michael P. Zaletel & Ali Yazdani. *Nature* **648**, 585–590 (2025).

The carrier-density/field relation is captured compactly by the **Středa formula** $\sigma_{xy} = e\,\partial n/\partial B$. The lesson — a topological insulator is an insulating bulk plus a conducting edge, with the quantum Hall system as the first example — is exactly the principle the rest of these notes develop.

III. Boundary Flow ⟷ Pump of Polarization

(**boundary** picture on the left, **bulk** picture on the right.)

On the left, the bulk bands (shaded) are bridged by an edge mode that flows across the gap as k_x sweeps the BZ; the Chern number is $c = 1$. On the right, the bulk Berry connection / Wannier center A_n^y rises smoothly from 0 to 1 as k_x traverses the zone — one quantum of charge is pumped. (That winding is the gauge-invariant **Wilson-loop spectrum**, made precise at the $t = 1$ endpoint below.) The two are

$$\textbf{topologically} \underline{\underline{=}} \textbf{equivalent} \tag{59}$$

Spectral flattening. The exact band energies are irrelevant to topology, so flatten them. Starting from

$$\hat{H}(k) = \sum_n \varepsilon_n(k)\,|\psi_{nk}\rangle\langle\psi_{nk}| \tag{60}$$

push every occupied energy to one constant and every empty energy to another:

$$\hat{H}(k) \;\longrightarrow\; \sum_n \varepsilon_{\text{Const}} \boxed{|\psi_{nk}\rangle\langle\psi_{nk}|} \tag{61}$$

so that, with $\hat{P}_{\text{occ}} = \sum_{occ} |\psi_n\rangle\langle\psi_n|$ the projector onto filled states,

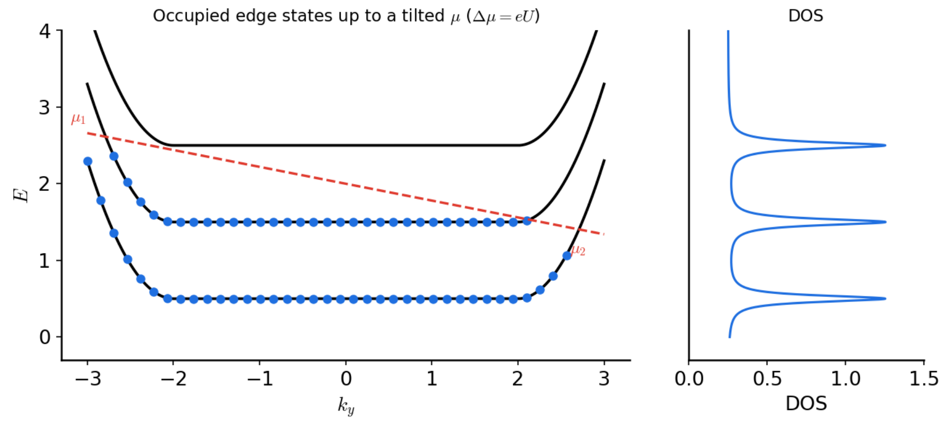

Figure 18. Edge spectrum: Landau levels flat in the bulk and bending up at the two boundaries; occupied states (filled dots) up to the tilted electrochemical potential, $\Delta\mu$ = eU between edges; DOS gapped in bulk, gapless at the edges

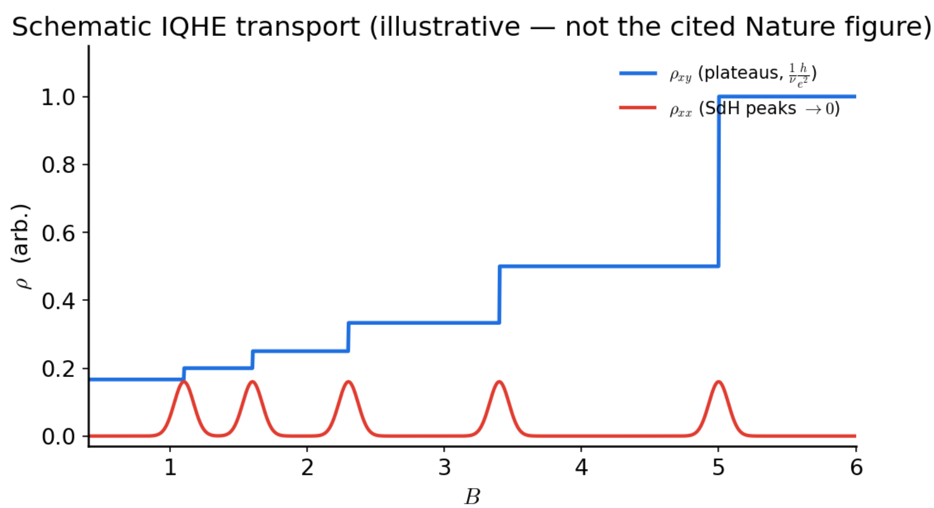

Figure 19. Schematic of the integer-quantum-Hall transport signature (illustrative redraw, not the cited Nature figure): ρ_xy quantized plateaus and ρ_xx Shubnikov–de Haas peaks collapsing to zero

$$\hat{H}^{\text{bulk}}_{\text{flat}} = 1 - 2\hat{P}_{\text{occ}}, \qquad \hat{P}_{\text{occ}} = \sum_{occ} |\psi_n\rangle\langle\psi_n| \tag{62}$$

(eigenvalues -1 on occupied states, $+1$ on empty states.)

Boundary Hamiltonian. Project a confining potential into the flattened problem:

$$\hat{H}^{\text{boundary}}_{\text{flat}} = \hat{P}\, V_0(\hat{y})\, \hat{P} + 1 - \hat{P} \tag{63}$$

$$V_0(\hat{y}) = \begin{cases} 1 & \text{outside } (y < 0) \\ -1 & \text{bulk } (y > 0) \end{cases} \tag{64}$$

Interpolate the step into a linear ramp with a parameter $t \in [0, 1]$ (shown at $t = \frac{1}{2}$):

$$V_t(y) = \begin{cases} -\dfrac{y}{t} & |y| < \dfrac{t}{1-t} \\ -\dfrac{\operatorname{sgn}(y)}{1-t} & |y| \geq \dfrac{t}{1-t} \end{cases} \tag{65}$$

At the kink $|y| = \dfrac{t}{1-t}$ both pieces equal $-\dfrac{\operatorname{sgn}(y)}{1-t}$, so V_t is **continuous**. It reduces to the sharp step $V_0 = -\operatorname{sgn}(y)$ as $t \to 0$ and to the linear ramp $V_1(y) = -y$ as $t \to 1$.

Analysis note (continuity correction). The handwritten plateau reads $-\operatorname{sgn}(y)$, which would make the linear piece overshoot to $-1/(1-t)$ at the kink and then jump down to -1. Matching the project's bulk–boundary note (the Fidkowski–Jackson–Klich interpolation, `content/posts/Bulk-Boundary-Correspondence`), the plateau must scale as $-\operatorname{sgn}(y)/(1-t)$ so that it meets the ramp continuously — the curves get *both* steeper and taller for smaller t. We use this continuous form.

At the endpoint $t = 1$ the projected boundary Hamiltonian becomes the projected position operator:

$$\hat{H}^{t=1} = -\hat{P}\,\hat{y}\,\hat{P} + 1 - \hat{P} \xrightarrow{\text{spectrum}} \langle\psi_n|\,\hat{y}\,|\psi_n\rangle \tag{66}$$

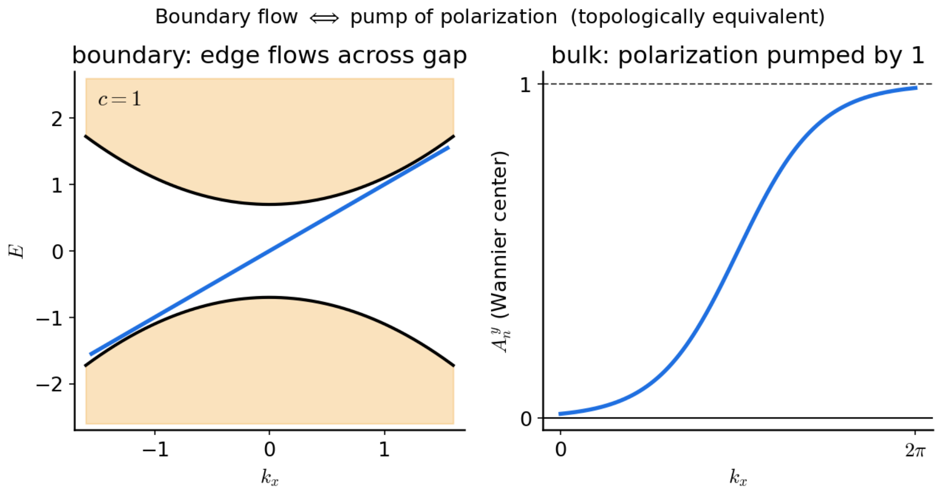

Figure 20. Left: boundary picture — an edge state (blue) flows across the bulk gap as k_x sweeps the Brillouin zone (Chern number c=1). Right: bulk picture — the Wannier center / Berry connection A_n^y winds from 0 to 1 over the zone (one pumped charge). The edge flow and the polarization pump are topologically equivalent.

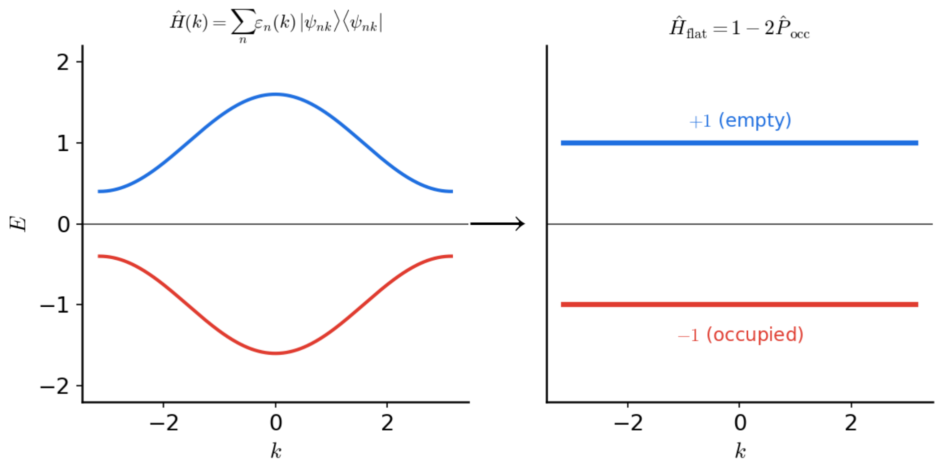

Figure 21. Spectral flattening: the dispersing valence/conduction bands are deformed to two flat levels at ±1 without closing the gap, so H_flat = 1 − 2P depends only on the projector onto occupied states.

These eigenvalues are exactly the **Wannier centers**: a maximally-localized Wannier function in a given direction is an eigenstate of the projected position operator $\hat{P}\hat{y}\hat{P}$. Under PBC the bare $\hat{y}$ is ill-defined, so one uses the unitary $\hat{Y} = \sum_{i\alpha} e^{-i\,\delta k_y R_i}|\alpha i\rangle\langle\alpha i|$ (position stored in a $U(1)$ phase, $\delta k_y = 2\pi/N_y$). At fixed k_x the projection $\hat{Y}_P = \hat{P}\hat{Y}\hat{P}$ is "screw-diagonal", its only nonzero blocks the overlaps $F^{mn}_{i,i+1} = \langle m, k_{y,i}|n, k_{y,i+1}\rangle$; multiplying them around the loop (transfer matrix) gives the **Wilson loop**

$$W(k_x) = \prod_i F_{i,i+1} = \mathscr{P}\exp\Big(-i\oint A_y(k)\,dk_y\Big), \qquad \bar{y}_n(k_x) = \frac{i}{2\pi}\ln\left[\text{eig}\,W(k_x)\right] \quad (\text{mod } 1), \tag{67}$$

a path-ordered exponential of the non-Abelian Berry connection $A_y^{mn} = i\langle m|\partial_{k_y}|n\rangle$. The winding of $\bar{y}_n(k_x)$ as k_x sweeps the BZ is precisely the Wannier-center flow — the bulk pump on the right of the figure — and equals the Chern number, computed gauge-invariantly (no numerical gauge fixing; Xi Dai *et al.*).

Analysis note (why this proves bulk–boundary correspondence). Flattening throws away all non-topological data, leaving only the projector $\hat{P}$. The boundary Hamiltonian $\hat{P}V(\hat{y})\hat{P} + (1-\hat{P})$ therefore has spectral flow that depends only on $\hat{P}$. Deforming the wall continuously ($V_0 \to V_t \to V_1$) cannot close the gap, so the number of in-gap

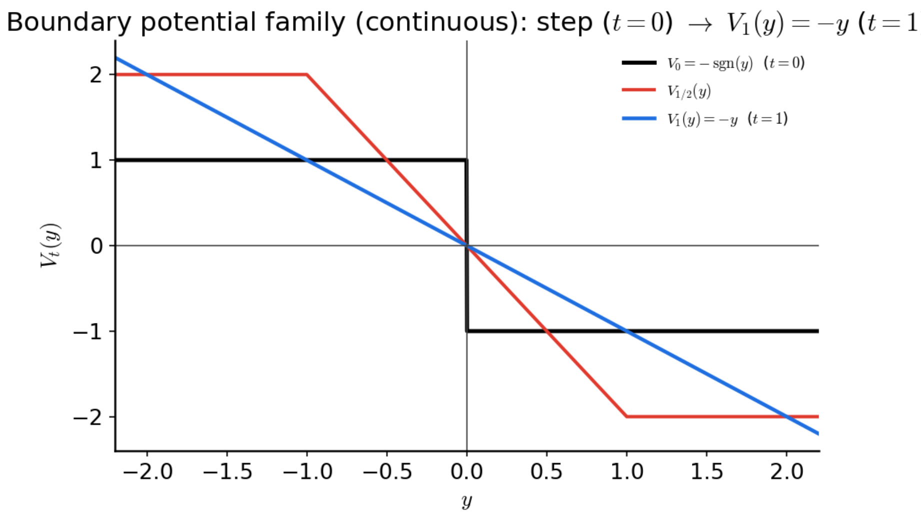

Figure 22. A family of boundary potentials V_t(y) interpolating from the sharp step V_0 = −sgn(y) at t=0, through V_{1/2}(y), to the full linear ramp V_1(y) = −y at t=1.

crossings is invariant: at $t = 0$ this is the **edge spectrum**, at $t = 1$ it is the **Wilson-loop / Wannier spectrum** $\langle\psi_n|\hat{y}|\psi_n\rangle = \int A_n\,dk$ (the bulk polarization), and the interpolation proves them topologically equivalent — the same number of gap-crossing branches with the same chirality (Fidkowski–Jackson–Klich). Hence *the number of times the edge mode flows across the gap = the winding of the bulk Wannier center = the Chern number*; "boundary flow" and "polarization pump" are two readings of the same integer. (The **entanglement spectrum** can be connected to the edge spectrum by the very same kind of interpolation — Turner–Zhang–Vishwanath, Qi *et al.* — giving yet another, boundary-free diagnostic of the topological edge.)

Continuing the $t = 1$ endpoint, acting with $\hat{H}^{t=1} = -\hat{P}\hat{y}\hat{P} + 1 - \hat{P}$ on an occupied state (writing $\hat{P} = |\psi_n\rangle\langle\psi_n|$):

$$\langle\psi_n|\Big(\,|\psi_n\rangle\langle\psi_n|\,\hat{y}\,|\psi_n\rangle\langle\psi_n| + 1 - |\psi_n\rangle\langle\psi_n|\,\Big)|\psi_n\rangle \qquad (68)$$

so the in-gap spectrum collapses onto the Wannier centers $\langle\psi_n|\hat{y}|\psi_n\rangle$, completing the bulk–boundary argument.

IV. Outlook: the topological zoo

A. 2D TI (Quantum Spin Hall)

A time-reversal-invariant insulator whose edge carries a **Kramers pair** of helical modes: spin-up and spin-down counter-propagate and cross protected by

$$\langle\psi|\,\hat{T}\,\psi\rangle = 0 \qquad (69)$$

(a state and its time-reverse are orthogonal — Kramers' theorem — so the crossing cannot gap out).

B. 3D TI

The surface hosts a single **Dirac cone** with spin–momentum locking: the spin winds once around the cone in the (k_x, k_y) surface BZ.

C. Weyl Semimetal

Gap-closing **Weyl nodes** act as Berry-curvature **monopoles**. Near a node the Hamiltonian is a 3D Weyl cone $H(\mathbf{q}) = \chi\,\hbar v\,\mathbf{q}\cdot\sigma$ with chirality $\chi = \pm 1$, and the Berry curvature is the field of a monopole sitting at the node, so a small enclosing sphere has Chern number

$$\oint_{S^2} \Omega \cdot d\mathbf{S} = \chi = \pm 1. \qquad (70)$$

The node is thus a **source** ($\odot$, $\chi = +1$) or **sink** ($\otimes$, $\chi = -1$) of Berry flux; nodes come in opposite-chirality pairs (Nielsen–Ninomiya). A 2D slice at fixed k_z *between* the nodes is a Chern insulator with $C = 1$, while outside the pair $C = 0$ — so C jumps by ± 1 as k_z crosses a node. By bulk–boundary correspondence each $C = 1$ slice carries one chiral edge state; stacking these over the range of k_z traces out an open **Fermi arc** that terminates exactly on the surface projections of the two nodes — a Fermi "surface" with endpoints, impossible in any purely 2D metal.

D. HOTI (Higher-Order Topological Insulator)

The bulk and ordinary surfaces are gapped, but topology is pushed to **lower-dimensional** boundaries: in d dimensions, protected modes appear on $(d-2)$-, $(d-3)$-, or even lower-dimensional boundaries instead of the usual $(d-1)$ — **hinge states** (1D modes on the edges of a 3D crystal) and **corner states** (0D modes at the corners of a 2D crystal). Equivalently, a $(d-1)$-dimensional face is itself a lower-dimensional topological insulator. The invariants are read off by **nested** Wilson loops / nested entanglement spectra — the same projector machinery of the previous page, applied one dimension down.

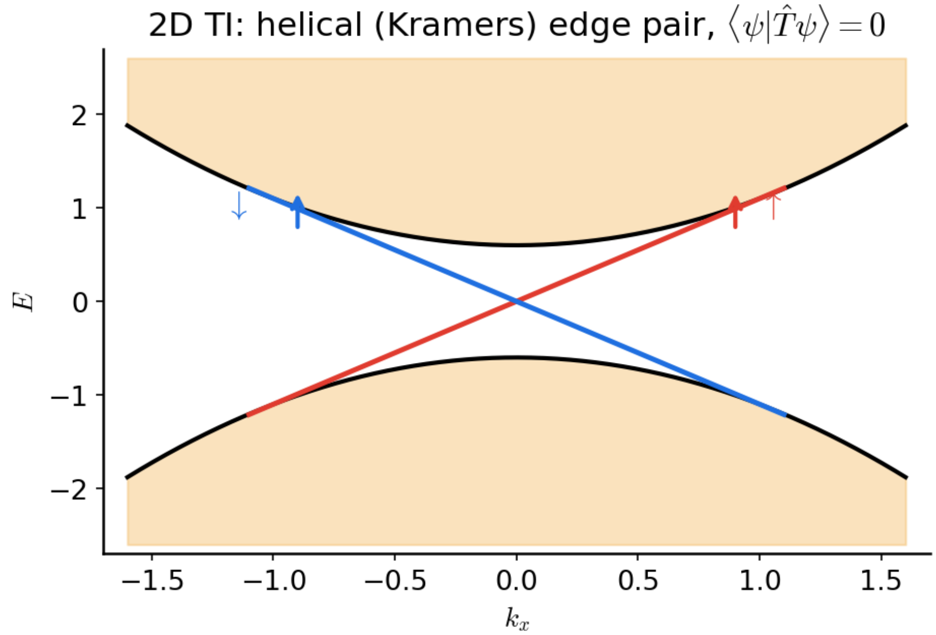

Figure 23. 2D topological insulator: bulk bands (black) bridged by a Kramers pair of helical edge states — spin-up (red, →) and spin-down (blue, ←) counter-propagate and cross at the time-reversal-invariant momentum.

Analysis note (the unifying thread). Every entry in this zoo is the same statement at a different symmetry/dimension: a bulk topological invariant forces protected boundary modes. For the Chern insulator it is $C \in \mathbb{Z}$ and chiral edges; for the **2D TI** it is the $\mathbb{Z}_2$ index protected by time reversal, giving helical (Kramers) edge pairs; for the **3D TI** it is a $\mathbb{Z}_2$ index giving an odd number of surface Dirac cones; for **Weyl semimetals** the invariant is the Chern number of a 2D slice between the nodes, which jumps by ± 1 across each node and produces Fermi arcs; for **HOTIs** the protected modes drop by more than one dimension (hinges, corners). Two refinements complete the picture. In a **topological crystalline insulator** the protecting symmetry is a crystal symmetry (e.g. a mirror), so protected modes survive only on boundaries that *preserve* it — a mirror-Chern insulator is gapless on mirror-symmetric edges and gapped on mirror-breaking ones (systematized by symmetry indicators / topological quantum chemistry over the 230 space groups). And in **fragile topology** the naive correspondence *fails*: the obstruction can be removed by adding trivial bands, so it is not one-to-one with edge states; the repair is a generalized correspondence under twisted boundary conditions (the gap must close as the twist completes a cycle), diagnosed by real-space invariants (Song *et al.*). In every case the seminar's logic — flatten the Hamiltonian, read the projector $\hat{P}$, count the boundary spectral flow — applies verbatim.

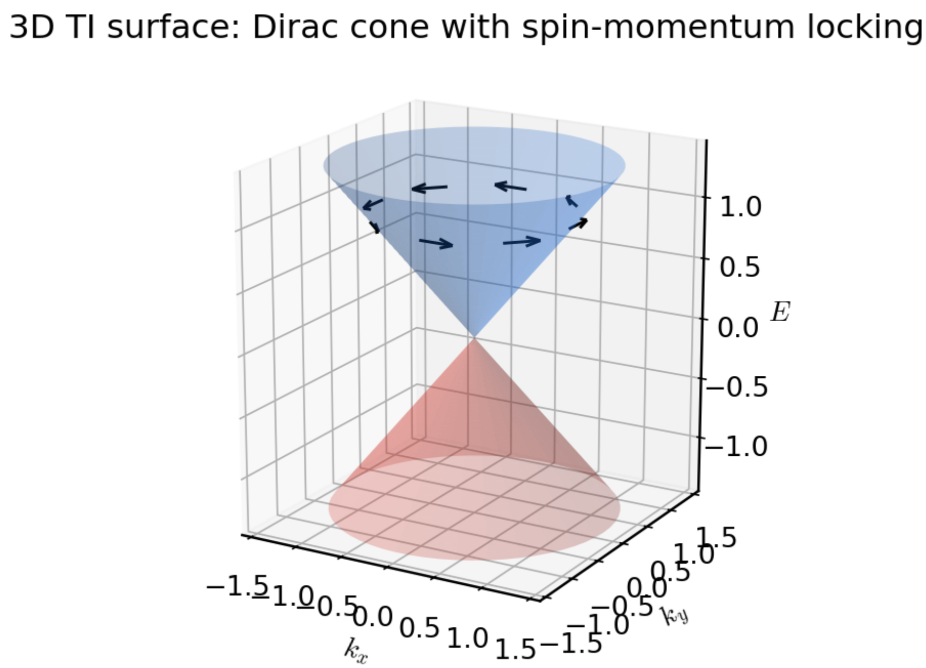

Figure 24. 3D topological insulator surface state: a single Dirac cone E(k_x,k_y) with the in-plane spin (arrows) locked perpendicular to momentum, winding once around the cone.

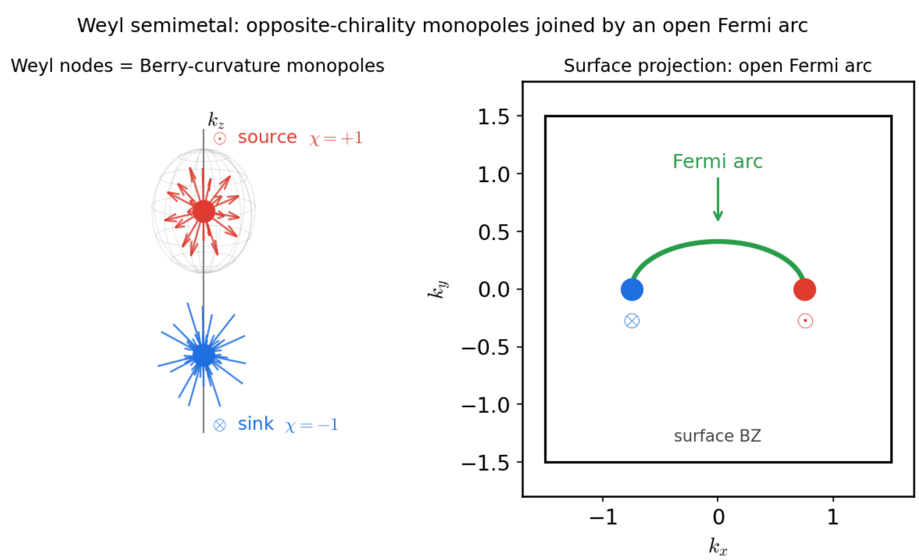

Figure 25. Weyl semimetal: a pair of opposite-chirality Weyl nodes — a Berry-flux source (⊙, χ=+1) and sink (⊗, χ=−1) at different k_z — with a Gauss sphere of Chern number ±1 around the source; their surface projections are joined by an open Fermi arc.

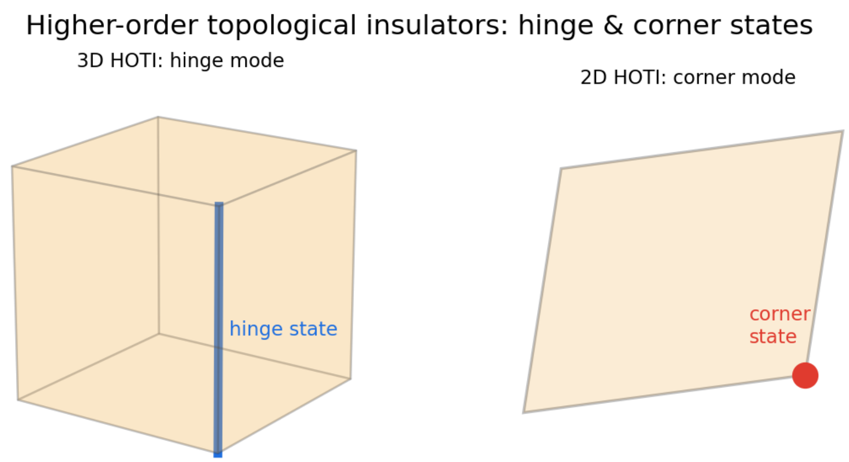

Figure 26. Higher-order topological insulator: a 3D crystal with a gapped bulk and gapped faces but a conducting hinge mode (blue) along one edge; and a 2D crystal with a localized corner state (red dot).